

A study of intense ionospheric scintillation observed during a quiet day in the East African low-latitude region

Chigomezyo M. Ngwira,^{1,2} Jeff Klenzing,² Joseph Olwendo,^{3,4} Florence M. D’ujanga,⁵ Russell Stoneback,⁶ and Paul Baki⁷

Received 16 February 2013; revised 15 May 2013; accepted 15 June 2013; published 6 August 2013.

[1] Ionospheric plasma density irregularities are a common feature of the equatorial and low-latitude ionosphere. These irregularities are known to cause fading and phase fluctuation (scintillation) of L-band radio navigation signals such as those used by Global Navigation Satellite Systems. This study investigates the occurrence of intense ionospheric scintillation in the postsunset period during a geomagnetically quiet day on 8 April 2011. In particular, we use Global Positioning System (GPS) derived observations, i.e., total electron content (TEC) and amplitude scintillation intensity index, S₄, to examine the occurrence of intense scintillations at two low-latitude stations in the East African sector. Deep TEC depletions, in some cases roughly 40 TECU, are observed consistently with the occurrence of intense scintillations. In addition, we compare the GPS-based observations to the Communication/Navigation Outage Forecasting System (C/NOFS) satellite plasma data. The intense scintillation events also correspond well with plasma depletion structures present on the C/NOFS observations and can be attributed to strong plasma bubble activity. The C/NOFS data also provide evidence of strong upward drift velocities (> 60 m/s) associated with the depletions, which may have contributed to the generation of the strong irregularities.

Citation: Ngwira, C. M., J. Klenzing, J. Olwendo, F. M. D’ujanga, R. Stoneback, and P. Baki (2013), A study of intense ionospheric scintillation observed during a quiet day in the East African low-latitude region, *Radio Sci.*, 48, 396–405, doi:10.1002/rds.20045.

1. Introduction

[2] Localized structuring of electron plasma density can occur when the ionosphere is perturbed. This is a typical feature of the equatorial *F* region ionosphere which becomes unstable under complex interaction between electric fields, neutral winds, and the Earth’s magnetic fields, particularly during the postsunset period [Basu *et al.*, 1999]. At such times, conditions may become favorable for the growth of instability mechanisms that lead to the development of ionospheric electron density irregularities. The presence of structured irregularities in the ionosphere can

cause fading and phase variation (scintillation) of L-band navigation signals such as those employed by Global Navigation Satellite Systems (GNSS) [see e.g., Aarons *et al.*, 1996; Basu *et al.*, 2002; Kintner *et al.*, 2007]. A typical example of such a system is the Global Positioning System (GPS).

[3] The equatorial and low-latitude ionosphere is one of the most extensively studied regions, as evidenced by widely documented literature [e.g., Kelley, 1989; Aarons, 1993; Kil *et al.*, 2002; De Paula *et al.*, 2003; Stolle *et al.*, 2006; Nishioka *et al.*, 2008; Adewale *et al.*, 2011; Ngwira *et al.*, 2013]. One of the notable features of this region is the occurrence of plasma density irregularities during geomagnetically quiet periods. Large-scale irregularities with typical east-west dimensions of several hundred kilometers are generated in the *F* region by various plasma processes involving an interchange of instabilities that include the Rayleigh-Taylor and $\mathbf{E} \times \mathbf{B}$ drift instability mechanisms [e.g., Kelley, 1989; Fejer *et al.*, 1999; De Paula *et al.*, 2007].

[4] After sunset, the eastward electric field \mathbf{E} along the dip equator is intensified due to conductivity gradients at the terminator via a process called the prereversal enhancement. The zonal electric field in the equatorial ionosphere is eastward during the day and is mapped from the *E* region to the *F* region [Heelis *et al.*, 1974; De Rezende *et al.*, 2007], producing an upward $\mathbf{E} \times \mathbf{B}/B^2$ drift velocity. The *F* region plasma at the dip equator is uplifted by the vertical $\mathbf{E} \times \mathbf{B}$ drift to higher altitudes, where it diffuses

¹Department of Physics, Catholic University of America, Washington, DC, USA.

²Space Weather Laboratory, NASA Goddard Space Flight Center, Greenbelt, Maryland, USA.

³Department of Mathematics and Physics, Pwani University College, Kilifi, Kenya.

⁴Department of Physics, University of Nairobi, Nairobi, Kenya.

⁵Department of Physics, Makerere University, Kampala, Uganda.

⁶W. B. Hanson Center for Space Sciences, University of Texas at Dallas, Richardson, Texas, USA.

⁷School of Pure and Applied Sciences, Kenya Polytechnic University College, Nairobi, Kenya.

Corresponding author: C. M. Ngwira, Space Weather Laboratory, NASA Goddard Space Flight Center, Greenbelt, MD 20771, USA. (chigomezyo.ngwira@nasa.gov or chigongwira@yahoo.co.uk)

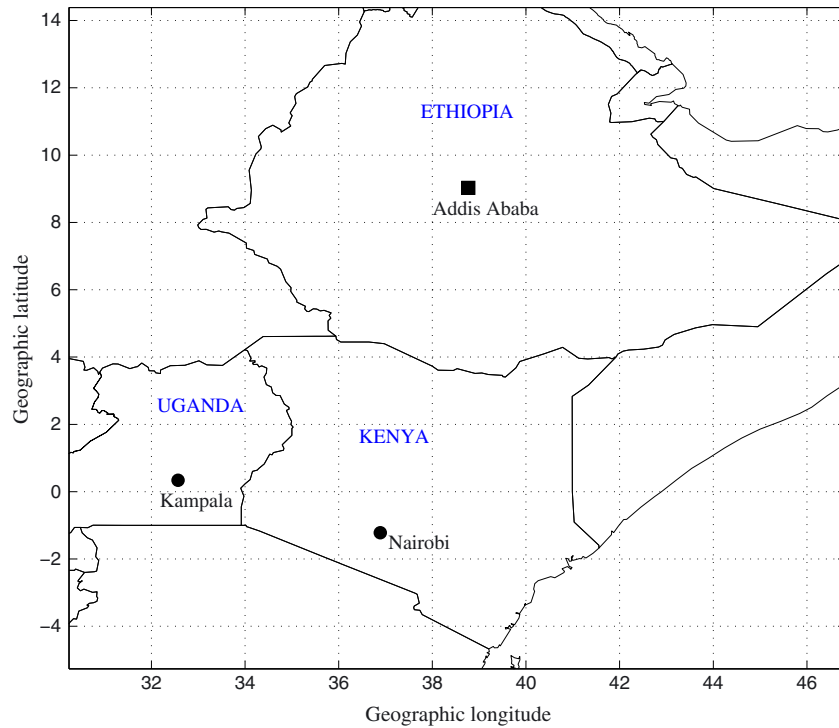


Figure 1. SCINDA (circles) ground receiver station locations used in this study. The location of Addis Ababa magnetometer station (square), which is along the dip equator, is also shown.

along magnetic field lines (by the action of gravity and the pressure gradient forces) leading to the development of the equatorial ionization anomaly (EIA) [Kelley, 1989]. The low-latitude irregularities cause intense scintillations along

the EIA, which are identified by the presence of electron density peaks observed between $\pm 18^\circ$ geomagnetic latitudes. Sharp upward plasma density gradients are created between the depleted bottomside ionosphere and the higher

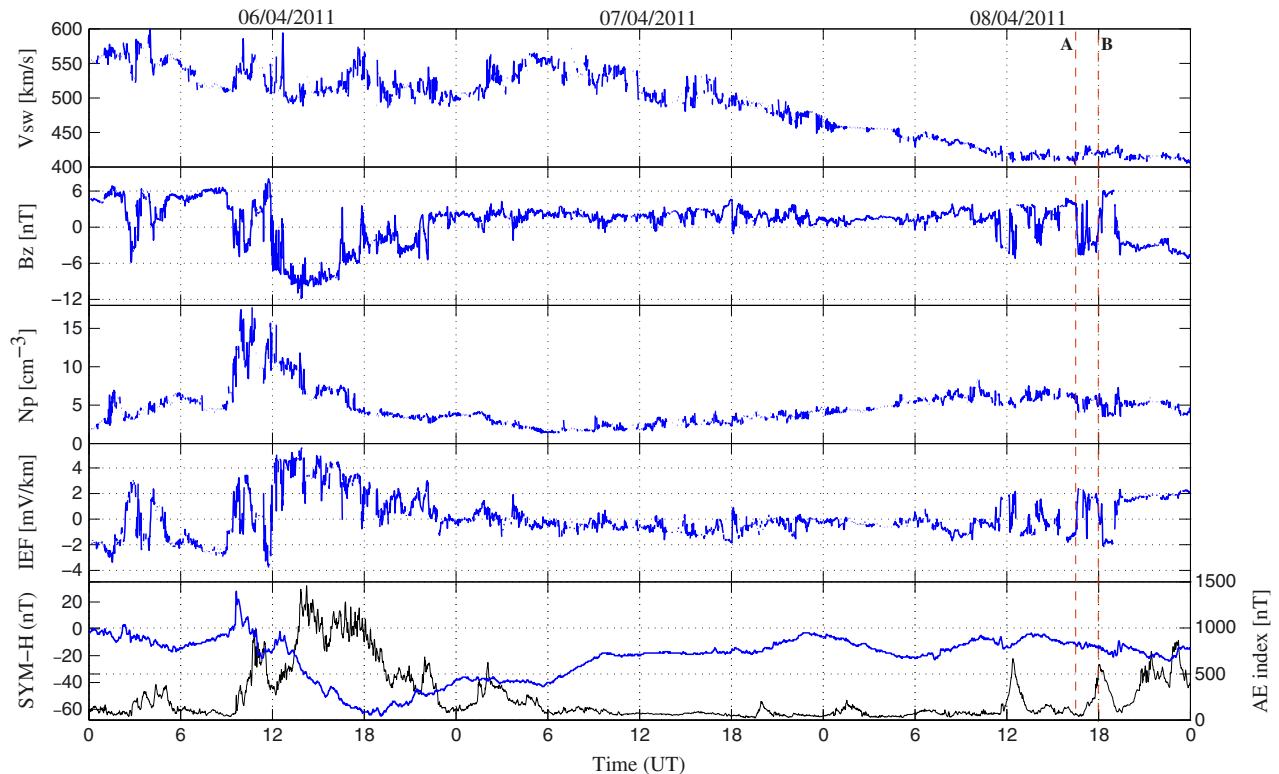


Figure 2. OMNI solar wind data and magnetometer derived geomagnetic indices for the period 6–8 April 2011.

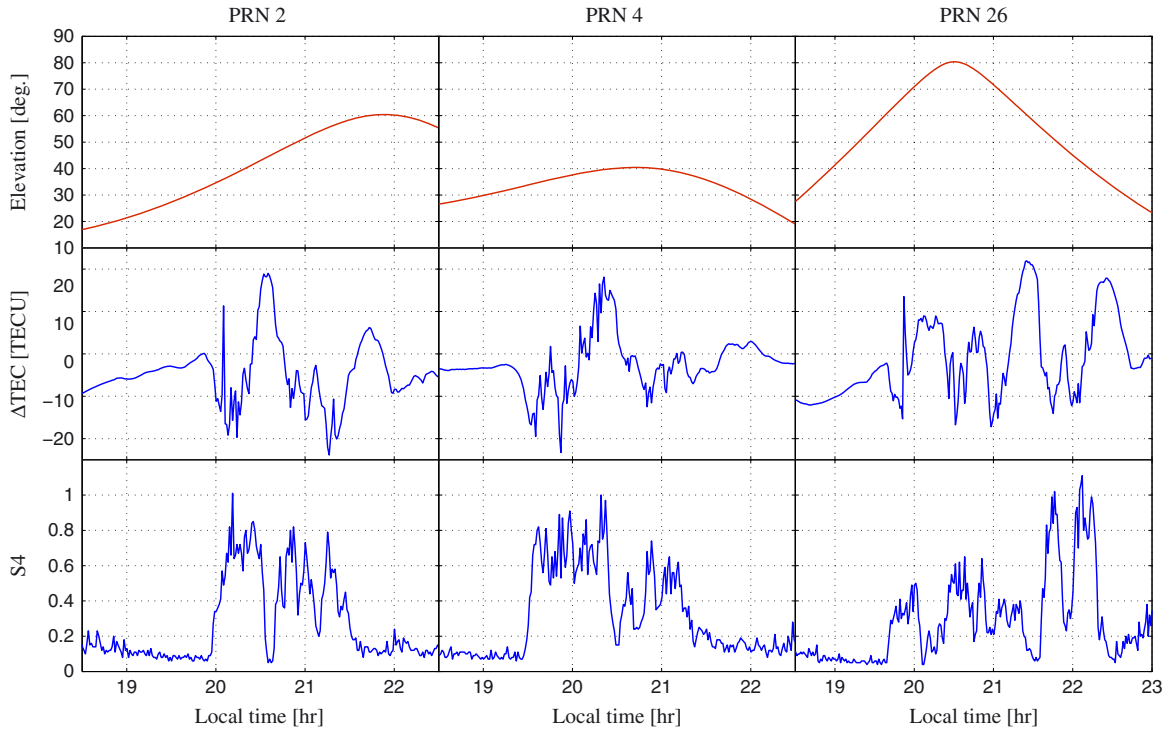


Figure 3. Examples of GPS TEC perturbations and scintillation measurements for three PRNs derived from the SCINDA ground station in Nairobi on 8 April 2011. The data are sampled at 1 min intervals. At this site, UT = local time – 2:27 h.

density in the topside F region that are known to be unstable to the development of plasma density instability mechanisms [Fejer *et al.*, 1999]. Thus, plasma descending from higher ionospheric heights fundamentally favors the generation

of equatorial irregularities. Under favorable ionospheric conditions, these irregularities can grow along geomagnetic field lines and are commonly referred to as plasma bubbles [De Paula *et al.*, 2007; Nishioka *et al.*, 2008].

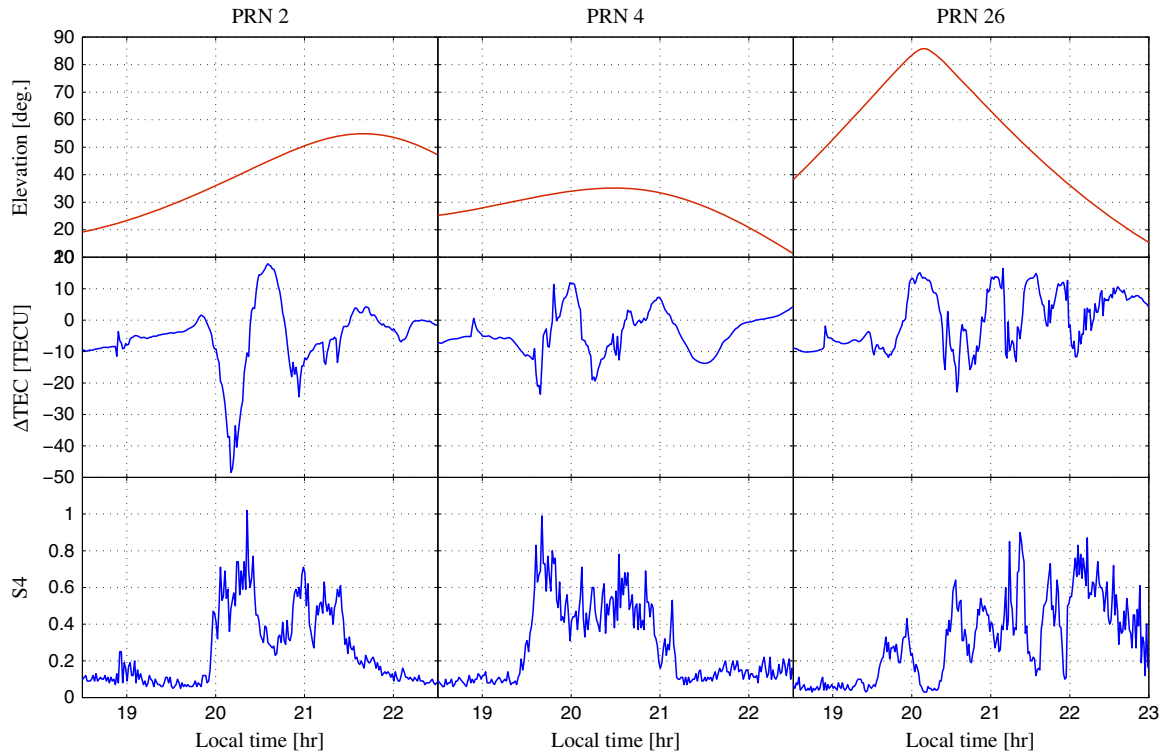


Figure 4. Same as Figure 3 but for the SCINDA ground station in Kampala on 8 April 2011. At this site, UT = local time – 2:10 h.

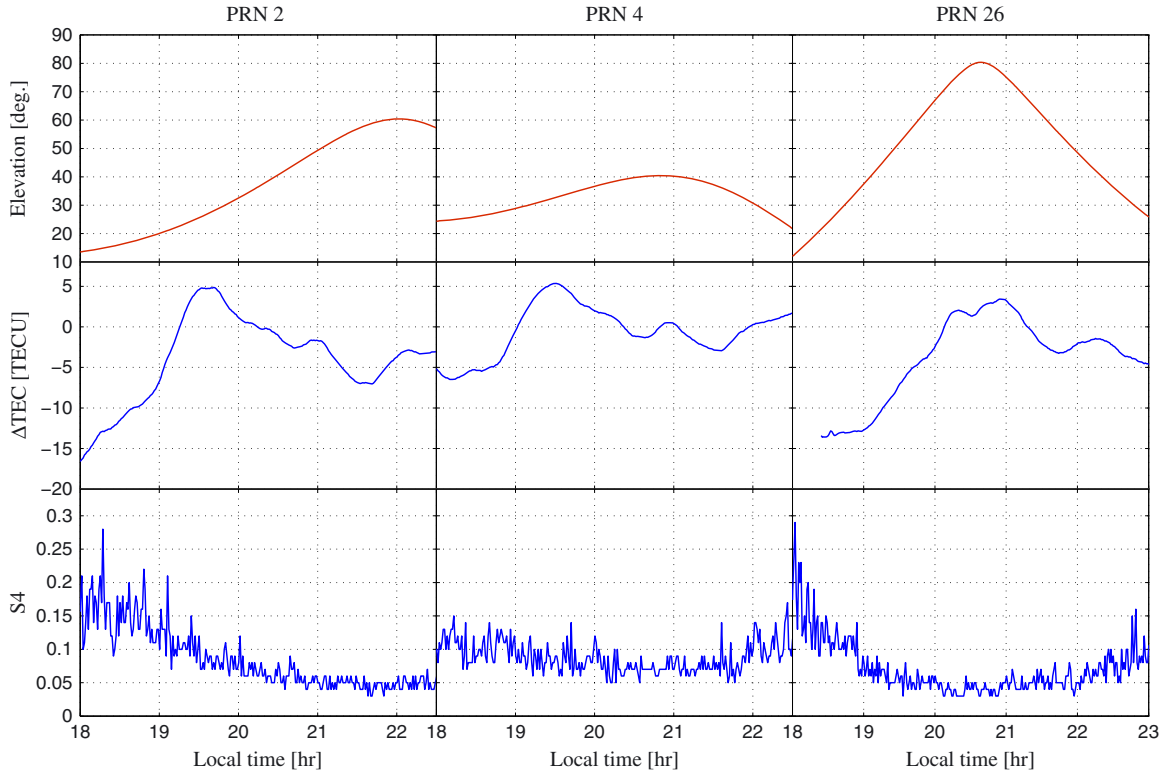


Figure 5. Examples of GPS TEC perturbations and scintillation measurements at Nairobi for measurements on 6 April 2011. No scintillations were observed on this day on the same PRNs as in Figure 3.

The occurrence of equatorial irregularities or scintillations is closely associated with local time, season, solar cycle, geomagnetic activity, and longitude of station.

[5] The ionosphere over Africa, which has the largest ground footprint along the geomagnetic equator, has not been well explored mainly due to the absence of ground-based ionospheric instrumentation across most of the continent [e.g., *Yizengaw et al.*, 2011; *Paznukhov et al.*, 2012]. However, many international collaboration efforts in the last 6 years have increased the availability of ground-based instrumentation over this previous unstudied region. The US Air Force Research Laboratory has deployed a ground-based network of SCINDA (Scintillation Network Decision Aid) receivers for the measurement of scintillations, irregularity drifts, and total electron content (TEC), specifically over the equatorial and low latitudes [e.g., *Groves et al.*, 1997]. Recently, a comprehensive study of equatorial plasma bubbles and L-band scintillations during solar minimum conditions was undertaken using several SCINDA receivers across Africa and has demonstrated that the ionosphere over Africa exhibits some unique irregularity patterns that are yet to be fully understood [e.g., *Paznukhov et al.*, 2012]. For example, these authors found that plasma bubbles occurred during all seasons of the year over the African sector, while they were not observed during some seasons in other longitude sectors.

[6] This study provides one of the first coordinated investigations of intense scintillation activity observed at two selected SCINDA network receivers in the East African sector. We employ a multi-instrument approach comprising

both space and ground-based measurements to probe the ionosphere over this region.

2. Data

[7] In the present paper, we investigated a case of intense scintillation observed on 8 April 2011. Two SCINDA network receivers sites, both operational since 2009, were used, i.e., Nairobi, Kenya (geographic: 1.27°S, 36.81°E; corrected magnetic latitude: 16.55°S) and Kampala, Uganda (geographic: 0.34°N, 32.57°E; corrected magnetic latitude: 15.60°S). The SCINDA ground station locations are shown on the map given in Figure 1.

[8] The Boston College GPS-TEC software [*Seemala and Valladares*, 2011] was used to derive TEC values and the amplitude scintillation intensity index (S4) from each SCINDA receiver observations. The S4 index is defined as the normalized ratio of the standard deviation of signal intensity fluctuations to the mean signal intensity. The GPS-TEC program uses the phase and code values for both L1 and L2 GPS frequencies to eliminate the effect of clock errors and tropospheric water vapor to calculate relative values of slant or line-of-sight TEC [*Sardón and Zarraga*, 1997]. The absolute values of TEC are obtained by including the differential satellite biases published by the University of Bern and the receiver bias that was calculated by minimizing the TEC variability between 02:00 and 06:00 LT. The equivalent vertical TEC at Ionospheric Pierce Point altitude of 350 km is calculated assuming the thin shell model

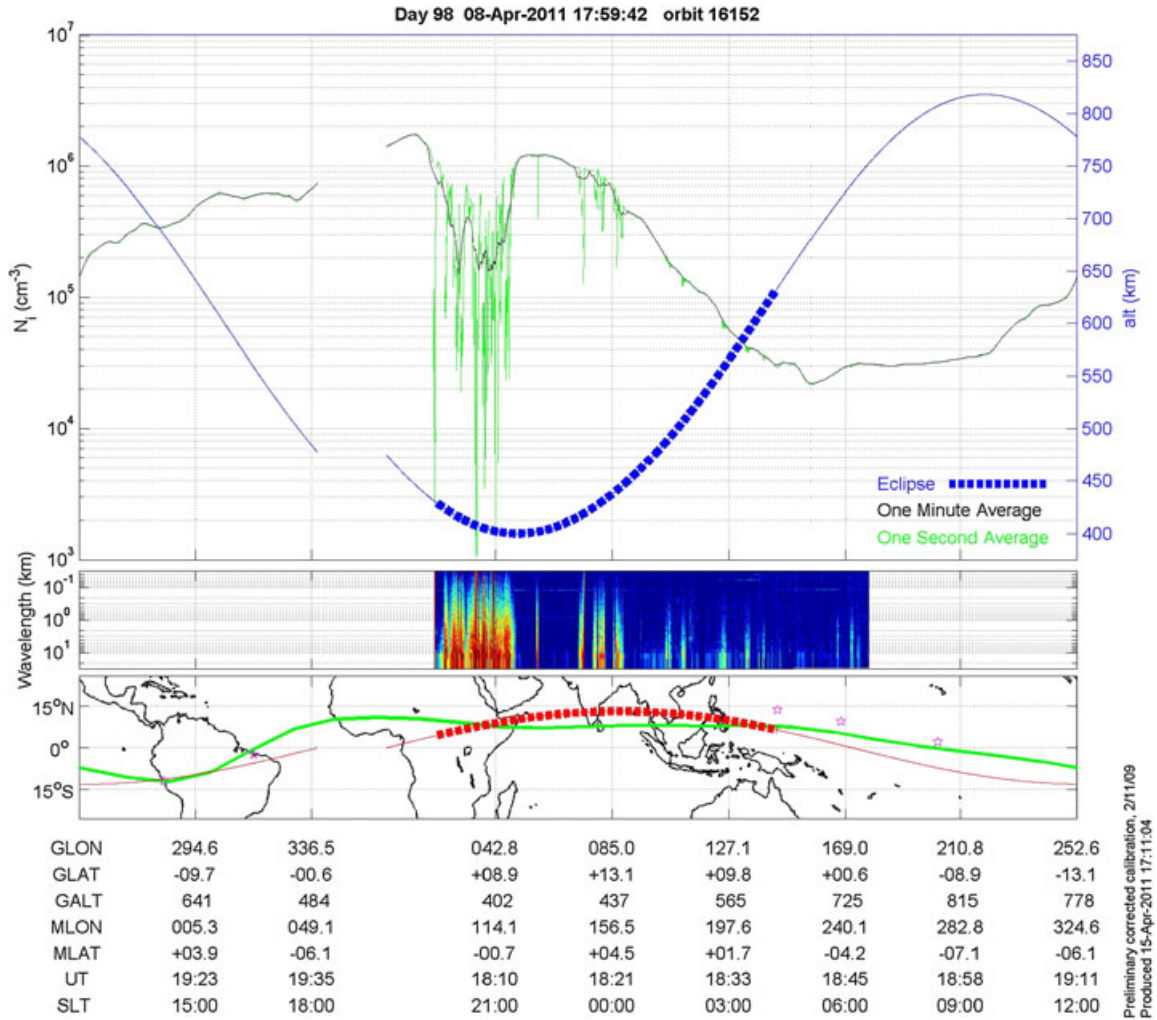


Figure 6. Postsunset plasma depletion on 8 April 2011. (top) 1 min integrated ionospheric density (black), 1 s integrated density (green), satellite altitude (blue). (middle) FFT from the 512 Hz PLP data. (bottom) Map with satellite trajectory (red) and geomagnetic equator (green).

[Coco *et al.*, 1991; Wilson and Mannucci, 1993; Ciraolo and Spalla, 1997, and references therein].

[9] In addition to the GPS observations, Communication/Navigation Outage Forecasting System (C/NOFS) satellite in situ measurements are used. The C/NOFS satellite was launched in April 2008 as part of a US Air Force mission to forecast ambient plasma densities and irregularities in the equatorial ionosphere that adversely impact communication and navigation systems. C/NOFS was launched into a low inclination (13°) orbit, with perigee of 400 km and apogee of 850 km, and was the first satellite entirely dedicated to forecasting ionospheric irregularities and radio wave scintillations. The satellite is equipped with sensors that measure different quantities including: plasma properties such as density and temperature; electric and magnetic fields; neutral winds; the strength of scintillation-producing irregularities; and electron content along the lines-of-sight between the C/NOFS and the GPS. Full details of the C/NOFS satellite instrumentation and science mission are discussed in the article by *de La Beaujardière et al.* [2004].

3. Observations

[10] The period of study presented in this paper corresponds to a geomagnetically quiet day (8 April 2011) during the ascending phase of the current solar cycle with moderate solar radio flux ($F_{10.7} = 109$), sunspot number = 97, and a maximum K_p index of 3. Solar wind and geomagnetic conditions corresponding to this day are presented in Figure 2. The figure shows from top to bottom: OMNI solar wind bulk velocity (V_{SW}), interplanetary magnetic field (IMF) B_z component, solar wind density, interplanetary electric field (IEF), and an over plot of the geomagnetic $SYM-H$ index (blue trace) and the AE index (black trace), respectively. The $SYM-H$ index is a high resolution (1 min) equivalent of the Dst index [Wanliss and Showalter, 2006]. As demonstrated by the $SYM-H$ index, there was a minor geomagnetic storm that started with a sudden impulse at $\sim 9:30$ UT on 6 April 2011, before gradually decreasing to a minimum $SYM-H$ index value of around -60 nT at 18:00 UT. This was immediately followed by a recovery phase. The geomagnetic conditions had returned to the prestorm levels in 8 April, ranging between -20 and -5 nT. On this

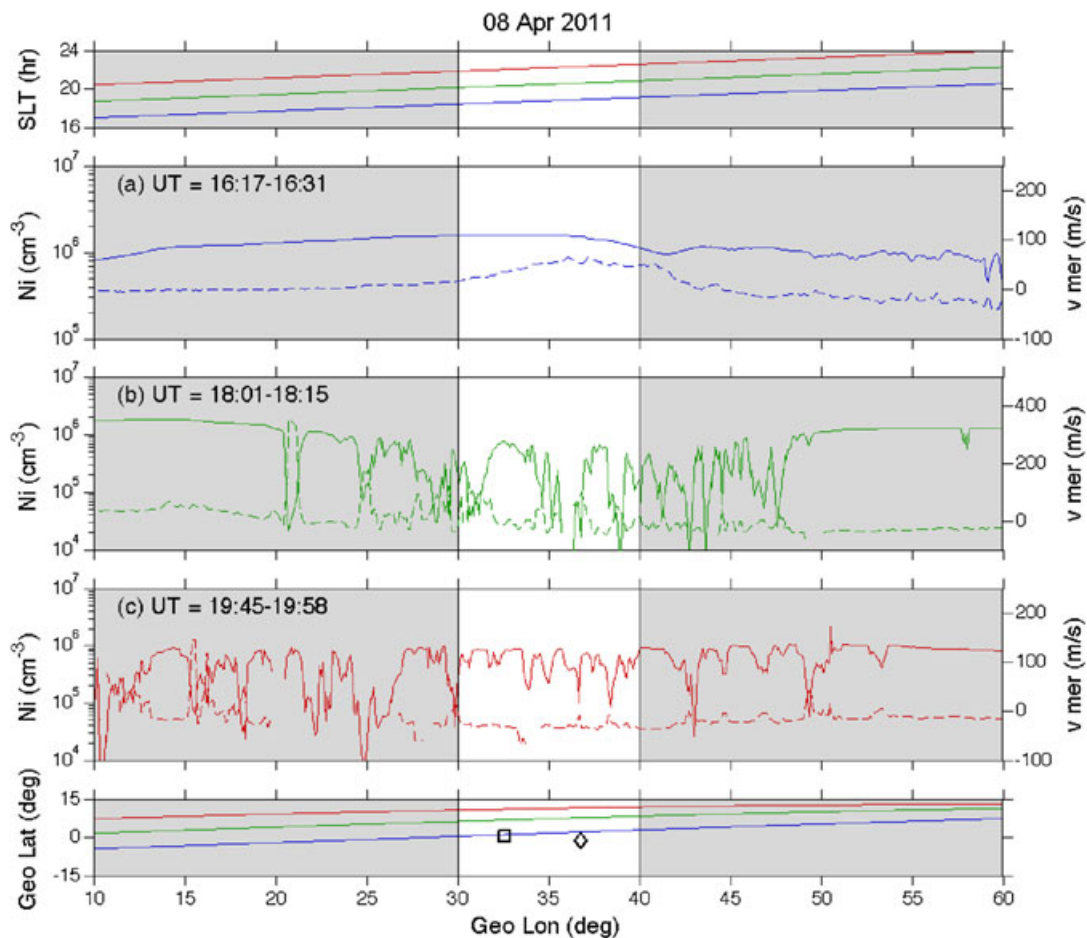


Figure 7. C/NOFS ion density (solid lines) and upward plasma drift (dashed lines) on 8 April 2011. The locations of the two ground stations at Kampala and Nairobi are marked in the bottom panel by the square and diamond, respectively.

same day, there were fairly stable interplanetary conditions except the IMF B_z component experienced some significant fluctuations between 16:00 and 22:00 UT. Notable among these fluctuations is the sudden reversal from a southward to a northward orientation at $\sim 18:00$ UT, turning from about -4 to 5 nT.

[11] In order to investigate the occurrence of scintillations, line-of-sight GPS-TEC data were used in addition to the S4 index. The GPS-TEC measurements were passed through a simple 15 min running mean filter. The filtered data were then subtracted from the original observations to determine the level of TEC perturbation (Δ TEC). With this approach, it is easier to see the TEC enhancements and depletions. Therefore, large-scale irregularity structures, which manifest as TEC depletions, can be examined.

[12] Presented in Figure 3 is the SCINDA data for the ground station at Nairobi during the postsunset period on 8 April 2011, while Figure 4 displays data for the ground station at Kampala during the same period. The figures show (top) the satellite elevation angle, (middle) TEC perturbations, and (bottom) amplitude scintillation intensity index S4 for the identified satellites. The scintillation events are presented for radio signals from PRNs (pseudorandom noise) 2, 4, and 26 for the two GPS ground receivers. For this study, only scintillation activity observed on satellites above 30°

of elevation was considered in order to reduce the effects of multipath.

[13] There are clear longitudinal differences between the observations in Figures 3 and 4. The two stations are separated by $\sim 4^\circ$ in longitude. Both TEC depletions (negative TECU) and TEC enhancements (positive TECU) are observed at both sites. The TEC enhancements have similar magnitudes at both sites, but the TEC depletions are much larger at Kampala than at Nairobi for PRN 2. However, the S4 levels are also comparable at both sites despite the large difference in the depth of depletions. It is possible that this effect may be due to the saturation of the S4 index. It is well known that under strong scattering conditions, the S4 index saturates to a value near unity, irrespective of the strength of the ionospheric perturbation [Carrano and Groves, 2010]. Both Figures 3 and 4 demonstrate good agreement between the level of S4 (bottom) and the depth of TEC perturbations (middle) in all cases and at each respective site. Clearly visible major TEC depletions (negative TECU) are observed with values as large as 20–40 TECU. The TEC depletions are also known as equatorial plasma bubbles or EPBs [e.g., Basu and Basu Su., 1981; Pi et al., 1997]. On the other hand, Figure 5 shows data for Nairobi during the postsunset period on 6 April 2011 when no scintillations were observed. As evident, there are no significant TEC perturbations on this

day, in particular TEC depletions, a sign that EPBs were not present.

[14] To probe the ionosphere from above, the Planar Langmuir Probe (PLP) on board the C/NOFS satellite takes measurements of the ambient ionospheric densities and electron temperatures. Further, it provides high temporal (512 Hz) and spatial resolution (~ 13 m) plasma density irregularity measurements. Additionally, the Ion Velocity Meter (IVM) provides measurements of the plasma density, composition, and the three-dimensional drift at 1 Hz. These drifts are rotated into the geomagnetic field-aligned frame. The meridional component is defined as the drift perpendicular to \mathbf{B} in the plane of the magnetic meridian. An upward $\mathbf{E} \times \mathbf{B}$ meridional drift corresponds to an eastward zonal electric field. Figure 6 reveals a deep plasma depletion containing small-scale density structures down to 100s of km observed in the postsunset period during C/NOFS orbit number 16152 around 18:10 UT on the day of interest at a satellite altitude of ~ 415 km. The ion density (solid lines) and velocity (dashed lines) measurements are depicted in Figures 7a–7c for three successive passes over the African low-latitude region. The ground footprint (bottom panel) of the three passes are located within about 10° northward of the SCINDA sites. Large ΔTEC negative structures occur around the same time that the depletions are seen on the SCINDA density observations in Figures 7a and 7b. The plasma density depletions are commonly observed at the C/NOFS satellite orbit altitudes and are related to scintillation activity [see e.g., *de La Beaujardière et al.*, 2009; *Nishioka et al.*, 2011].

4. Discussions

[15] We have presented the ionospheric conditions associated with the development of intense scintillations at two low-latitude ground stations in the East African sector. It is well known that the nonlinear development of a large spectrum of irregularities of different scale-sizes can be investigated by various observational techniques [*Cervera and Thomas*, 2006, and references therein]. At GPS carrier frequencies, it is possible to detect EPBs, which typically appear as plasma depletion structures on the TEC data.

[16] According to current understanding, it is generally believed that deeper depletions are responsible for stronger scintillations, given that the scintillation intensity is directly proportional to the electron density variations along the GPS radio signal path [e.g., *Fremouw et al.*, 1980; *Steenburgh et al.*, 2007]. This is clearly illustrated in both Figures 3 and 4 (middle panels) that show large plasma density depletions corresponding to intense scintillation activity. A recent study of equatorial bubbles and L-band scintillations during solar minimum (2010) by *Paznukhov et al.* [2012] revealed that the depth of depletions did not exceed 7 TECU. However, we notice here depletion structures with depths ranging between 5 and 40 TECU. This is not surprising since we are looking at events during an ascending phase of the solar cycle when background densities become higher due to increasing solar activity [see e.g., *Huang et al.*, 2002]. The depletion structures are a manifestation of bubbles, and often embedded within them are the small-scale irregularities responsible for scintillations [*Basu et al.*, 1999; *Cervera and Thomas*, 2006]. *Whalen* [2009] attempted to quantify

scintillation in terms of electron density and was of the view that even though scintillation is attributed to EPBs, its strength is strongly controlled by the background electron density that the bubble intersects, as a higher background density can trigger larger density fluctuations. This is well reflected in the Fast Fourier Transform (FFT) of PLP ion density data that is provided as color spectrogram in the middle panel of Figure 6. The FFT basically reveals large-amplitude irregularities within the postsunset depletions [*de La Beaujardière et al.*, 2009]. Further evidence in support of higher background electron density is offered by *Basu and Groves* [2001] who found scintillation to be greater at the anomaly peaks than at the dip equator by simultaneous measurements in both locations using the SCINDA network.

[17] The initial C/NOFS orbit pass in Figure 7a does not show any depletions in the near vicinity of the ground stations, though the corresponding IVM drift velocity shows a prereversal enhancement with a peak of ~ 65 m/s. However, the subsequent passes (Figures 7b and 7c) show a series of depletions extending from about 10° to 50°E longitude with the deepest depletions at least two orders of magnitude less than the background density. A comparison of the ground-based receiver observations to the C/NOFS plasma density measurements provided in Figure 7 shows that the time of occurrence of TEC depletions and S4 activity is consistent with the observations of density structures from C/NOFS. Furthermore, our ground observations illustrate that the scintillation activity started to develop in the postsunset period and terminated before local midnight, while the C/NOFS data demonstrate that the density depletions are well correlated with the corresponding IVM upward $\mathbf{E} \times \mathbf{B}$ drift velocity measurements. A well-developed prereversal electric field, as inferred from the upward vertical drift velocity of the equatorial F layer, is believed to be the primary cause of the $\mathbf{E} \times \mathbf{B}$ drift velocity [e.g., *Fejer et al.*, 1999; *Whalen*, 2001] and is one of the major conditions associated with onset of early-evening irregularities.

[18] In Figure 8, we provide C/NOFS measurements for 6 April 2011, which show no enhancement of the prereversal drift velocity. This figure also shows that no ion density depletions were present between 30° and 40° of geomagnetic longitude, a region corresponding to the location of the two stations. The development of the prereversal enhancement drift velocity on this day was probably suppressed by the storm as seen in Figure 2.

[19] *Fejer et al.* [1999] observed that when the prereversal enhancement drift velocities were sufficiently large, the necessary seeding mechanisms for the development of strong Spread F irregularities appeared to be ever present. There is clear evidence of a large prereversal drift velocity (~ 65 m/s) that is seen on the C/NOFS data provided in Figure 7 for 8 April. One mechanism that can explain the enhancement of the prereversal drift velocity on 8 April is the penetration of magnetospheric electric fields to lower latitudes, which can occur in response to rapid IMF-driven changes in the strength of magnetospheric convection [*Kikuchi et al.*, 2000; *Fejer et al.*, 2007]. As evident in Figure 2, the IMF B_z component and the associated IEF experienced some significant rapid fluctuations between 16:00 and 22:00 UT as marked by the two vertical dashed lines A and B. A comparison of Figures 2 and 7 shows that the drift velocity (Figure 7a) started to increase around about the same time that

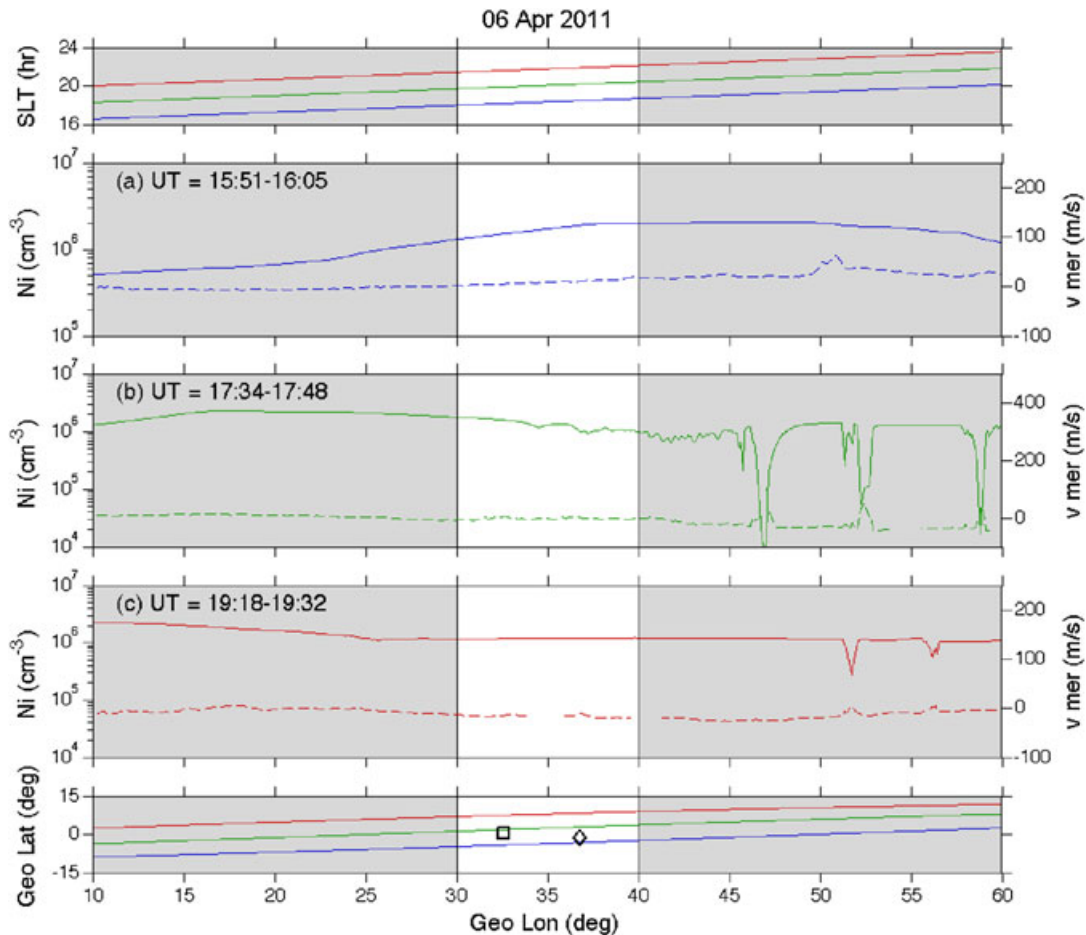


Figure 8. Same as Figure 7 but for C/NOFS ion density and upward plasma drift on 6 April 2011.

fluctuations are observed on the IMF B_z component. A penetration eastward electric field can lift equatorial plasma upward due to $\mathbf{E} \times \mathbf{B}$ drift so that more plasma is available at higher altitudes where recombination rates are low. This may also help to explain the intense amplitude scintillations ($S_4 \sim 1$), as large drift velocities in-turn ensure strong and fully developed EIA peaks that lead to well-developed irregularities [Whalen, 2001].

[20] An interesting feature of the scintillation pattern at both sites investigated here is the long duration associated with the high level activity ($S_4 > 0.5$). In some cases, the high level activity lasts well over an hour. This is not unique to these observations and is consistent with earlier published results that used data from SCINDA ground receivers [see e.g., Groves *et al.*, 1997; Paznukhov *et al.*, 2012; Olwendo *et al.*, 2012]. The long duration could be caused by the persistent occurrence of EPBs and indicates that irregularity generation may have continued for several hours. The C/NOFS satellite repeatedly observed deep plasma density depletions during two passes (Figures 7b and 7c) that were separated in time by approximately 2 h. Note that for pass c (Figure 7c), the irregularities span a longitude covering roughly 3 h of local time. According to Basu *et al.* [2001], fresh generation of irregularities can be related to the disturbance dynamo generated eastward electric field. Figure 2 shows a sudden northward turning of the IMF at $\sim 18:00$ UT

(vertical line B) that is accompanied by an enhancement of the AE index. This could have provided a contribution to the disturbance dynamo effect. However, there is need to further investigate the total contribution of the disturbance dynamo and other mechanisms, such as neutral winds, toward the generation of these irregularities.

5. Summary

[21] Using a multi-instrument approach, we discussed the development of intense scintillations that occurred on 8 April 2011 at two low-latitude stations in the East African sector. We found significant longitudinal differences between the two sites in terms of the TEC depletion levels, but the level of scintillations were comparable for both sites. This effect contradicts observations from earlier studies such as Paznukhov *et al.* [2012] and needs to be explored in greater detail. However, by comparing observations from ground-based SCINDA receivers to C/NOFS satellite measurements, we have established that the intense levels of scintillation were driven by significantly deep plasma bubble activity. The strong plasma bubbles were probably generated with the help of an enhanced eastward electric field, as revealed in the C/NOFS plasma drift measurements, which ensured that there was more plasma available at higher altitudes. A high background density is an essential requirement

for the development of strong irregularities that give rise to larger magnitude of scintillations [e.g., Basu et al., 2001; Basu and Groves, 2001; Nishioka et al., 2011].

[22] While this study is not the first to use a combination of SCINDA receivers and C/NOFS data to investigate scintillations, it is apparently the first of its kind carried out over the African sector. Given the limited data resources in this sector at the present time, it is still not possible to clearly identify the driving mechanism(s) associated with the strong scintillations. However, this study highlights significant longitudinal variations in East Africa and should encourage continued work in this region. Therefore, the present study reveals some of the major challenges of exploring the dynamics of the equatorial ionosphere over Africa by showing that more ground instrumentation is still needed to effectively investigate the African sector.

[23] **Acknowledgments.** We would like to acknowledge Prof. Patricia Doherty from Boston College for her support toward this work. We thank the various international cooperating partners for the GPS-SCINDA ground instrument support. The authors acknowledge Patrick Roddy for the C/NOFS PLP plot, and the instrument designer, John Ballenthin. The solar wind data were obtained through the CDAWeb database, which is hosted by the NASA/GSFC Space Physics Data Facility.

References

- Aarons, J. (1993), The longitudinal morphology of equatorial F-layer irregularities relevant to their occurrence, *Space Sci. Rev.*, *63*, 209–243.
- Aarons, J., M. Mendillo, and R. Yantosca (1996), GPS phase fluctuations in the equatorial region during the MISETA 1994 campaign, *J. Geophys. Res.*, *101*(A12), 26,851–26,862.
- Adewale, A. O., E. O. Oyejeme, A. B. Adeyoye, C. M. Ngwira, and R. Athieno (2011), Response of the equatorial F region to different geomagnetic storms observed by GPS in the African sector, *J. Geophys. Res.*, *116*, A12319, doi:10.1029/2011JA16998.
- Basu, S., and Su. Basu (1981), Equatorial scintillations—a review, *J. Atmos. Terr. Phys.*, *43*(5/6), 473–489.
- Basu, S., and K. M. Groves (2001), Specification and forecasting of outages on communication/navigation and navigation systems, in *Space Weather: Geophys. Monogr. Ser.*, vol. 125, edited by D. Song, H. J. Singer, and G. L. Siscoe, pp. 423–430, AGU, Washington, D. C.
- Basu, S., K. M. Groves, Su. Basu, and P. J. Sultan (2002), Specification and forecasting of scintillations in communication/navigation links: Current status and future plans, *J. Atmos. Sol.-Terr. Phys.*, *64*, 1745–1754.
- Basu, S., K. M. Groves, J. M. Quinn, and P. Doherty (1999), A comparison of TEC fluctuations and scintillations at Ascension Island, *J. Atmos. Sol.-Terr. Phys.*, *61*(16), 1219–1226.
- Basu, S., et al. (2001), Ionospheric effects of major magnetic storms during the International Space Weather Period of September and October 1999: GPS observations, VHF/UHF scintillations, and in situ density structures at middle and equatorial latitudes, *Geophys. Res. Lett.*, *106*(A12), 30,389–30,413.
- Carrano, C. S., and K. M. Groves (2010), Temporal decorrelation of GPS satellite signals due to multiple scattering from ionospheric irregularities, *Proceedings of the 23rd International Technical Meeting of The Satellite Division of the Institute of Navigation (ION GNSS 2010)*, Portland, OR, September 2010, pp. 361–374.
- Cervera, M. A., and R. M. Thomas (2006), Latitudinal and temporal variation of the equatorial ionospheric irregularities determined from GPS scintillation observations, *Ann. Geophys.*, *24*, 3329–3341.
- Ciraolo, L., and P. Spalla (1997), Comparison of ionospheric total electron content from the Navy Navigation Satellite System and the GPS, *Radio Sci.*, *32*, 1071–1080.
- Coco, D., C. Coker, S. R. Dahlke, and J. R. Clynch (1991), Variability of GPS satellite differential group delay biases, *IEEE Trans. Aerosp. Electron. Syst. Lausanne*, *27*, 931–938.
- de La Beaujardière, O., et al. (2004), C/NOFS: A mission to forecast scintillations, *J. Atmos. Sol.-Terr. Phys.*, *66*(17), 1573–1591, doi:10.1016/j.jastp.2004.07.030.
- de La Beaujardière, O., et al. (2009), C/NOFS observations of deep plasma depletions at dawn, *Geophys. Res. Lett.*, *36*, L00C06, doi:10.1029/2009GL038884.
- De Paula, E. R., F. S. Rodrigues, K. N. Iyer, I. J. Kantor, P. M. Kintner, B. M. Ladvinia, and H. Kil (2003), Equatorial anomaly effects on GPS scintillations in Brazil, *Adv. Space Res.*, *31*(3), 749–754.
- De Paula, E. R., et al. (2007), Characteristics of the ionospheric F-region plasma irregularities over Brazilian longitudinal sector, *Indian J. Radio Sci.*, *36*(4), 268–277.
- De Rezende, L. F. C., E. R. De Paula, I. S. Batista, I. J. Kantor, and M. T. De Assis Honorato Muella (2007), Study of ionospheric irregularities during intense magnetic storms, *Braz. J. Geophys.*, *25*(Supl. 2), 151–158.
- Fejer, B. G., L. Scherliess, and E. R. de Paula (1999), Effects of the vertical plasma drift velocity on the generation and evolution of equatorial spread F, *J. Geophys. Res.*, *104*(A9), 19,859–19,869.
- Fejer, B. G., J. W. Jensen, T. Kikuchi, M. A. Abdu, and J. L. Chau (2007), Equatorial ionospheric electric fields during the November 2004 magnetic storm, *J. Geophys. Res.*, *112*, A10304, doi:10.1029/2007JA012376.
- Fremouw, E. J., R. C. Livingston, and D. A. Miller (1980), On the statistics of scintillating signals, *J. Atmos. Terr. Phys.*, *42*, 717–731.
- Groves, K. M., et al. (1997), Equatorial scintillation and systems support, *Radio Sci.*, *32*(5), 2047–2064.
- Heelis, R. A., P. C. Kendall, R. J. Moffett, D. W. Windle, and H. Rishbeth (1974), Electrical coupling of the E- and F-region and its effect on F-region drifts and winds, *Planet. Space Sci.*, *22*, 743–756.
- Huang, C.-S., J. C. Foster, L. P. Goncharenko, P. J. Erickson, W. Rideout, and A. J. Coster (2002), Equatorial plasma bubbles observed by DMSP satellites during a full solar cycle: Towards a global climatology, *J. Geophys. Res.*, *107*(A12), 1434, doi:10.1029/2002JA009452.
- Kelley, M. C. (1989), *The Earth's Ionosphere*, 487 pp., Academic Press, London.
- Kikuchi, T., H. Lüehr, K. Schlegel, H. Tachihara, M. Shinohara, and T.-I. Kitamura (2000), Penetration of auroral electric fields to the equator during a substorm, *J. Geophys. Res.*, *105*(A10), 23,251–23,261.
- Kil, H., P. M. Kintner, E. R. de Paula, and I. J. Kantor (2002), Latitudinal variations of scintillation activity and zonal plasma drifts in South America, *Radio Sci.*, *37*(1), 6-1–6-7, doi:10.1029/2001RS002468.
- Kintner, P. M., B. M. Ledvinia, and E. R. de Paula (2007), GPS and ionospheric scintillations, *Space Weather*, *5*, S09003, doi:10.1029/2006SW000260.
- Ngwira, C. M., G. K. Seemala, and J. B. Habarulema (2013), Simultaneous observations of ionospheric irregularities in the African low-latitude region, *J. Atmos. Sol.-Terr. Phys.*, *97*, 50–57, doi:10.1016/j.jastp.2013.02.014.
- Nishioka, M., A. Saito, and T. Tsugawa (2008), Occurrence characteristics of plasma bubble derived from global ground-based GPS receiver networks, *J. Geophys. Res.*, *113*, A05301, doi:10.1029/2007JA012605.
- Nishioka, M., Su. Basu, S. Basu, C. E. Valladares, R. E. Sheehan, P. A. Roddy, and K. M. Groves (2011), C/NOFS satellite observations of equatorial ionospheric plasma structures supported by multiple ground-based diagnostics in October 2008, *J. Geophys. Res.*, *116*, A10323, doi:10.1029/2011JA016446.
- Olowendo, J. O., P. J. Cilliers, P. Baki, and C. Mito (2012), Using GPS-SCINDA observations to study the correlation between scintillation, total electron content enhancement and depletions over the Kenyan region, *Adv. Space Res.*, *49*, 1363–1372.
- Paznukhov, V. V., et al. (2012), Equatorial plasma bubbles and L-band scintillations in Africa during solar minimum, *Ann. Geophys.*, *30*, 675–682.
- Pi, X., A. J. Mannucci, U. J. Lindqwister, and C. M. Ho (1997), Monitoring of global ionospheric irregularities using the worldwide GPS network, *Geophys. Res. Lett.*, *24*(18), 2283–2286.
- Sardón, E., and N. Zarraoa (1997), Estimation of total electron content using GPS data: How stable are the differential satellite and receiver instrumental biases? *Radio Sci.*, *32*(5), 1899–1910.
- Seemala, G. K., and C. E. Valladares (2011), Statistics of total electron content depletions observed over the South American continent for the year 2008, *Radio Sci.*, *46*, RS5019, doi:10.1029/2011RS004722.
- Steenburgh, R. A., C. G. Smithro, and K. M. Groves (2007), Ionospheric scintillation effects on single frequency GPS, *Space Weather*, *6*, S04D02, doi:10.1029/2007SW000340.
- Stolle, C., H. Lüehr, M. Rother, and G. Balasis (2006), Magnetic signatures of equatorial spread F as observed by the CHAMP satellite, *J. Geophys. Res.*, *111*, A02304, doi:10.1029/2006JA011184.
- Wanliss, J. A., and K. M. Showalter (2006), High-resolution global storm index: Dst versus SYM-H, *J. Geophys. Res.*, *111*, A02202, doi:10.1029/2005JA011034.
- Whalen, J. A. (2001), The equatorial anomaly: Its quantitative relation to equatorial bubbles, bottomside spread F, and $\mathbf{E} \times \mathbf{B}$ drift velocity during a month at solar maximum, *J. Geophys. Res.*, *106*(A12), 29,125–29,132.

- Whalen, J. A. (2009), The linear dependence of GHz scintillation on electron density observed in the equatorial anomaly, *Ann. Geophys.*, *27*, 1755–1761.
- Wilson, B. D., and A. J. Mannucci (1993), Instrumental biases in ionospheric measurements derived from GPS data, *Proceedings of the Institute of Navigation GPS-93*, Washington, D. C., pp. 1343–51.
- Yizengaw, E., M. B. Moldwin, A. Mebrahtu, B. Dامتie, E. Zesta, C. E. Valladares, and P. Doherty (2011), Comparison of storm time equatorial ionospheric electrodynamics in the African and American sectors, *J. Atmos. Sol.-Terr. Phys.*, *73*(1), 156–163, doi:10.1016/j.jastp.2010.08.008.